ACS APPLIED NANO MATERIALS

www.acsanm.org Article

# Nanolayered Heterostructures of N-Doped $TiO_2$ and N-Doped Carbon for Hydrogen Evolution

Xianglong Kong, Zhenbo Peng, Rui Jiang, Peipei Jia, Jing Feng, Piaoping Yang,* Qianqian Chi, Wei Ye,* Fuchun Xu, and Peng Gao*

Cite This: *ACS Appl. Nano Mater.* 2020, 3, 1373−1381 Read Online

ACCESS | Metrics & More | Article Recommendations | Supporting Information

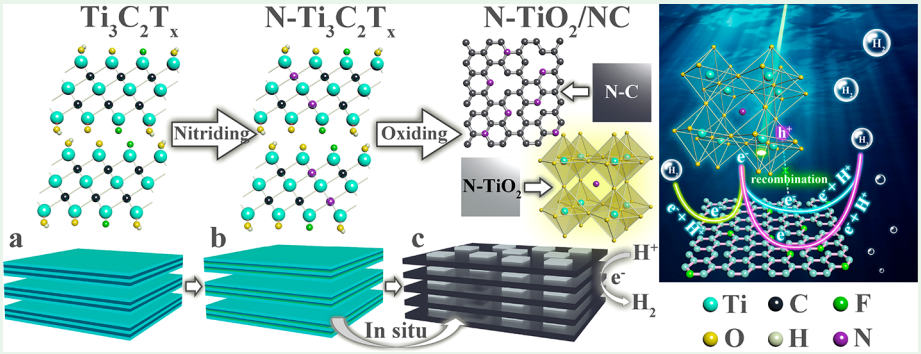


**ABSTRACT:** Both doping and compositing in $TiO_2$ are exceedingly effective strategies to overcome the compound's shortcomings, such as invalid visible-light response and enormous recombination of photogenerated carriers. Herein, a convenient and cost-effective route has been put forward to in situ synthesize nanolayered heterostructure based on N-doped $TiO_2$ nanoparticles and N-doped carbon (N-$TiO_2$/NC) using 2D layered N-MXene (N−$Ti_3C_2T_x$) as the template. The as-obtained N-$TiO_2$/NC nanocomposite displays greatly enhanced visible light absorption property, superior carrier separation and transport ability. As a result, the nanolayered N-$TiO_2$/NC heterostructure exhibits a satisfactory $H_2$ evolution rate from water-splitting (102.6 $\mu$mol $g^{-1}$ $h^{-1}$) under visible-light without any additional cocatalyst. The study provides a new strategy for the synthesis of defective nanoheterostructure and expands the applications of MXene family.

**KEYWORDS:** *$TiO_2$, carbon, MXene, N-doping, photocatalytic $H_2$ evolution*

## 1. INTRODUCTION

Converting solar energy into clean energy, such as hydrogen energy, is admitted as one of the most effective approaches to resolve the severe energy crisis and the emerging environmental pollution problem.[1−3] Water is pushed in front of humans as an initiation and termination for hydrogen utilizing through a simple catalytic decomposition reaction.[4,5] As a typical hot spot in burgeoning photocatalysts for water splitting, $TiO_2$ has been widely considered as a promising material because of its abundant reserves and relatively excellent photocatalytic ability.[6−8] However, individual $TiO_2$ has a wide band gap (3.2 eV for anatase) and a high photoexcited carrier recombination rate (~90% within 10 ns), which hinders its practical application.[9−12] Over the past decades, a large quantity of exploring works based on defect engineering have been carried out to promote the compound's light absorption and carrier separation properties. Nonmetallic ions (C, N, S) doping is one of the defect engineering strategies to adjust the band positions.[13−16] Particularly, N doping is widely studied due to its preferable visible light response and high $H_2$ production rate.[17−19] Just like every coin has two sides, N-doping also creates enormous recombination centers of photogenerated electrons and holes, resulting in the debasement for photocatalytic activity.[20,21] Therefore, a lightweight conductive supporter is needed to realize the spatial electron−hole separation, such as carbon material family.[22−24] However, individual carbon material lacks suitable sites for adsorption of active H· and $H_2$ evolution. Hence, many valuable efforts around doping have been executed. Particularly, nitrogen-doped carbon materials are considered an excellent strategy for improving its conductivity and ability of $H_2$ production.[25,26] However, compared to the preparation of $TiO_2$ by using $Ti(OC_4H_9)_4$ and the preparation of $TiO_2$ and carbon composite by traditional physical adsorption methods, we applied nitriding MXene and in situ growth to synthesize doped $TiO_2$/C composite.[27−29] The nanolayered heterostruc-

**Received:** November 12, 2019
**Accepted:** January 28, 2020
**Published:** January 28, 2020







https://dx.doi.org/10.1021/acsanm.9b02217
*ACS Appl. Nano Mater.* 2020, 3, 1373−1381

**Scheme 1. Preparation Process for $Ti_3C_2T_x$-MXene, N-$Ti_3C_2T_x$, and N-$TiO_2$/NC Heterostructure**

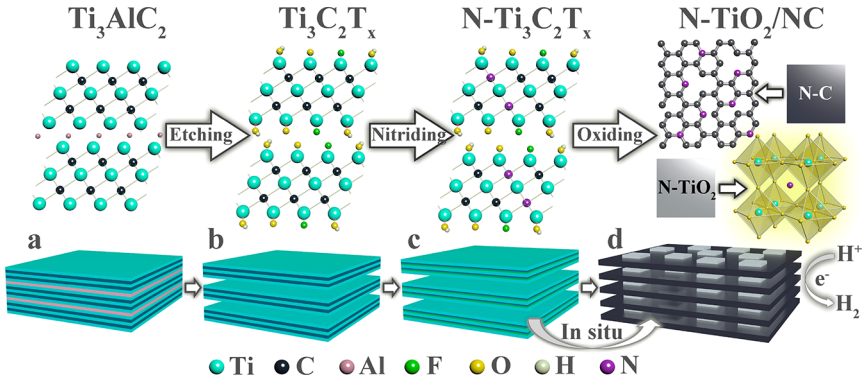


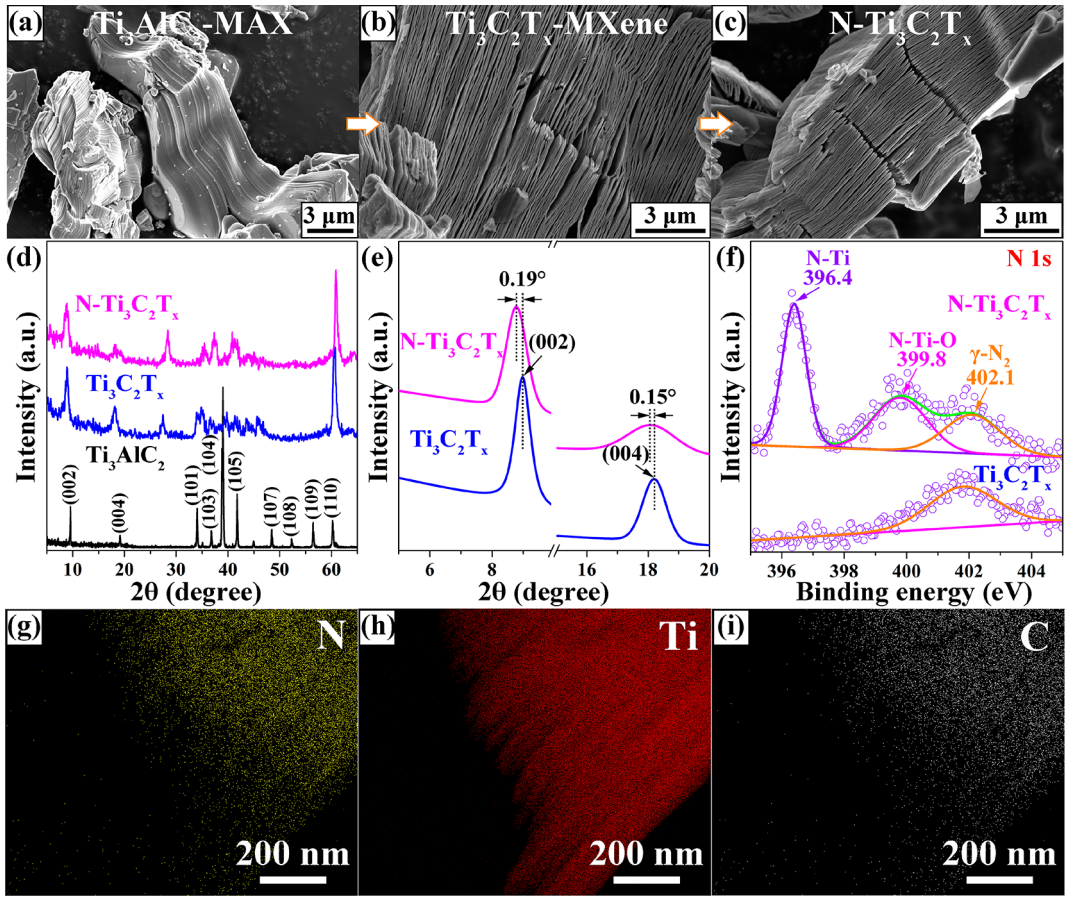


**Figure 1.** SEM images of (a) $Ti_3AlC_2$-MAX, (b) $Ti_3C_2T_x$-MXene, and (c) N−$Ti_3C_2T_x$. (d) XRD patterns, (e) enlarged (002) peak and (004) peak, and (f) N 1s XPS spectra of the $Ti_3C_2T_x$ and N−$Ti_3C_2T_x$ samples. (g−i) STEM EDS mappings of N−$Ti_3C_2T_x$: (g) N, (h) Ti, and (i) C.

ture of N-$TiO_2$/NC presents excellent orderliness and the intimate connection between $TiO_2$ and carbon, which is beneficial to the improvement of charge transfer and photocatalytic performance.

Recently, 2D MXenes, consisting of transition metal carbide or nitride, have shown excellent electrical performance and have been applied in many research fields, such as catalysts and Li-ion battery.[30−34] Recently, several research groups have reported that N-doped $Ti_3C_2T_x$ by a hydrothermal method or heat treatment using urea or $NH_3$ as nitrogen source exhibits a better stability and superior electrochemical performance.[35−37] In addition, because of their unique electrical properties, MXene members have been identified as the cocatalysts with the most potential. $Ti_3C_2$ MXene-based composites, such as g-$C_3N_4$@$Ti_3C_2$ QDs, $Ti_3C_2$/$TiO_2$ nanoflowers, $Ti_3C_2$@$TiO_2$@$MoS_2$, $Ti_3C_2$/$TiO_2$/1T-$MoS_2$, Cu/$TiO_2$@$Ti_3C_2T_x$, and $Cu_2O$/(001)$TiO_2$@$Ti_3C_2T_x$, exhibit prominent photocatalytic $H_2$ production performance.[38−43] In order to obtain N-doped $TiO_2$ and defect carbon composite, in this work, we selected $Ti_3C_2T_x$ MXene as the C and Ti resource and the 2D skeleton for the following stacked heterostructure.

In view of the above analysis, we have successfully applied a convenient route to synthesize nanolayered photocatalyst of N-doped $TiO_2$ nanoparticles and N-doped C derived from layered N-MXene for the first time. This process involves two steps: (1) N-doped $Ti_3C_2T_x$ (N−$Ti_3C_2T_x$), which provides a


https://dx.doi.org/10.1021/acsanm.9b02217
ACS Appl. Nano Mater. 2020, 3, 1373−1381

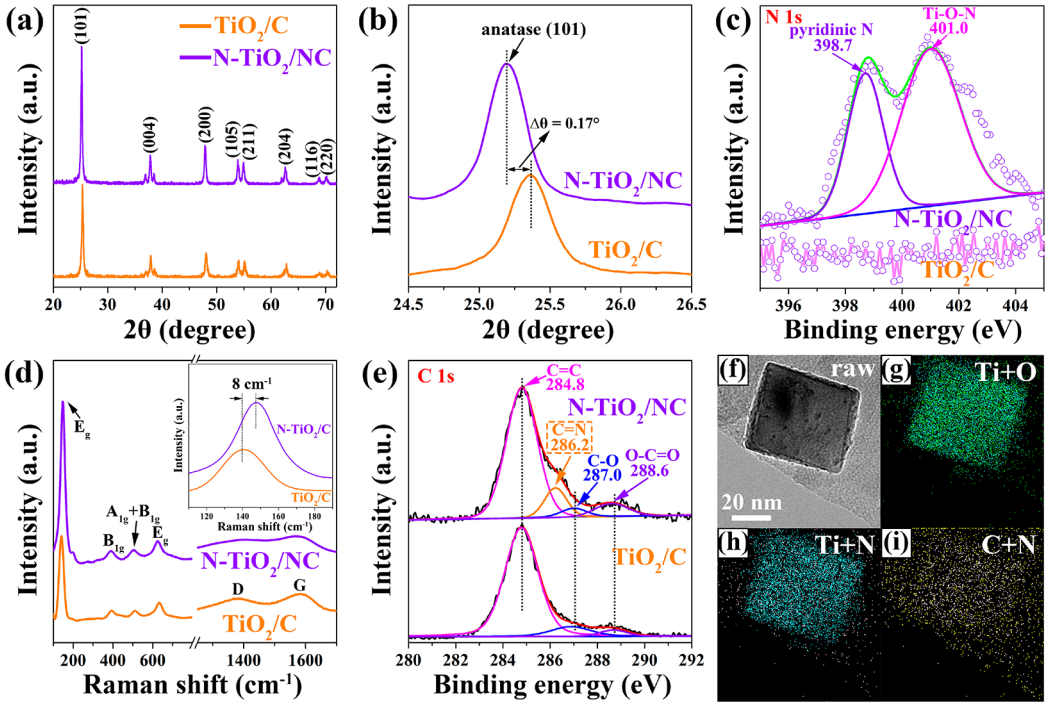


**Figure 2.** (a) XRD patterns and (b) enlarged (101) peaks of $TiO_2$/C and N-$TiO_2$/NC samples; (c) N 1s XPS spectra, (d) C 1s XPS spectra and (e) FTIR spectra of $TiO_2$/C and N-$TiO_2$/NC; (f–i) HAADF-STEM image of N-$TiO_2$/NC and its corresponding EDS graph. Element color: Ti (blue), O (green), C (yellow), and N (pink).

laminated skeleton and a nitrogen source for the next procedure; 2) oxidation of N–$Ti_3C_2T_x$, which results in the formation of stacked heterostructure consisted of N-$TiO_2$ nanocrystals and N doped carbon, as shown in Scheme 1. The laminated N-$TiO_2$/NC nanoheterostructure could robustly separate photoexcited carrier and transfer more photoelectrons into suitable reaction sites, thus promoting the mass production of hydrogen by water decomposition. The as-obtained N-$TiO_2$/NC with nanolayered heterostructure exhibits an outstanding $H_2$ evolution rate up to 102.6 $\mu$mol $g^{-1}$ $h^{-1}$ under visible light without any additional cocatalyst. The method for N-doping of $TiO_2$ and carbon based on 2D laminated materials provides a novel insight for defective semiconductor nanohybrids.

## 2. EXPERIMENTAL SECTION

**2.1. Preparation of $Ti_3C_2T_x$-MXene.** $Ti_3AlC_2$ powder (1 g) was divided into multiple portions and then slowly added to HF (49%, 10 mL). The above suspension was placed in a magnetic stirrer and maintained at 40 °C for 36 h. After reaction, the mixture was washed with deionized water by multiple high-speed centrifugation (at a speed of 5000 rpm) until the pH of the supernatant was approximately 7 as measured by a pH meter. The centrifuged "clay" ($Ti_3C_2T_x$-MXene) was kept at 60 °C for 24 h in a vacuum oven.

**2.2. Preparation of N-Doped $Ti_3C_2T_x$.** The above as-prepared $Ti_3C_2T_x$ MXene powder was transferred into a tube furnace and kept in argon gas stream for 1 h. After that, the tube furnace was continuously fed with ammonia gas (100 mL $min^{-1}$) for 2 h at 450 °C.

**2.3. Preparation of N-$TiO_2$/NC and $TiO_2$/C Samples.** The N-$TiO_2$/NC sample are obtained through the following steps. N–$Ti_3C_2T_x$ powder was placed in alumina boat. The above alumina boat was rapidly (approximately 3 s) pushed into the center of a tube furnace that had been preheated to 530 °C (10 °C $min^{-1}$) for 4 min. The alumina boat was rapidly (approximately 3 s) was quickly removed from the tube furnace and transferred to a vacuum box for natural cooling to room temperature. The $TiO_2$/C sample was synthesized in the same condition, in which only N–$Ti_3C_2T_x$ was replaced by $Ti_3C_2T_x$.

## 3. RESULTS AND DISCUSSION

The morphologies of $Ti_3AlC_2$-MAX, $Ti_3C_2T_x$-MXene, and N–$Ti_3C_2T_x$ samples were first observed by SEM measurements, as exhibited in Figure 1a–c and Figure S1a, b. It is seen in Figure 1b and Figure S1b that obvious stacked layer structure is embodied after HF etching $Ti_3C_2T_x$-MXene. Interestingly, N–$Ti_3C_2T_x$ (Figure 1c) after ammonia treatment maintains almost the same layered structure as $Ti_3C_2T_x$ (Figure 1b). It is observed (Figure 1d, e) that the XRD peaks of nitrogen-doped $Ti_3C_2T_x$ have slight shifts compared with pristine $Ti_3C_2T_x$. This result may be duo to lattice distortion induced by the N-doping. Figure 1f and Table S1 show the N 1s XPS spectra and corresponding peak analyses of $Ti_3C_2T_x$ before and after ammonia treatment. The appearance of N–Ti bond at 396.6 eV and N–Ti–O bond at 399.8 eV indicates that heterogeneous N atoms are successfully induced into MXene and partial N atoms replace the position of carbon in $Ti_3C_2T_x$.[32,33] The peak at 402.1 eV in $Ti_3C_2T_x$-MXene is attributed to chemisorbed $N_2$. The XPS results, C 1s XPS spectra and corresponding peak analyses of $Ti_3C_2T_x$ and N–$Ti_3C_2T_x$ (Figure S2 and Table S2 and S3) also prove the N-replacing. The intensity of C–Ti bond and C/Ti atom ratio in N-$Ti_3C_2T_x$ are significantly lower than those of pristine $Ti_3C_2T_x$, which implies that partial C–Ti bonds are converted to N–Ti chemical bonds. From STEM EDX mapping of N-MXene (Figure 1g–i and Figure S3a–c), it is obviously found that the nitrogen element is evenly distributed on MXene and the same phenomenon occurs with other elements. This again identifies the successful introduction of nitrogen. The above


https://dx.doi.org/10.1021/acsanm.9b02217
ACS Appl. Nano Mater. 2020, 3, 1373–1381

results confirmed that nitrogen-doped MXene is successfully synthesized by us.

To analyze the converting process, we carried out a series of time-dependent experiments on the change of MXene. It is clearly observed from XRD patterns and C 1s and Ti 2p XPS spectra (Figure S4−S6) that the characteristic peak of anatase $TiO_2$ and Ti−C bond in $Ti_3C_2T_x$-MXene disappear completely, and the Ti $2p_{3/2}$ and Ti $2p_{1/2}$ present after heating the $Ti_3C_2T_x$ powder for 4 min in air. It can be found (Figure S7) that more $TiO_2$ particles on the MXene appear as the oxidation time increased and eventually fully cover the layers. The above results indicate that $Ti_3C_2T_x$-MXene is completely converted to $TiO_2$ and carbon after heating for 4 min in air. So the oxidation time of N-doped MXene and $Ti_3C_2T_x$-MXene is 4 min. Many test results also proved that unreacted N-MXene did not appear in the N-$TiO_2$/NC sample, as exhibited in Figure S8. It is observed in Figure S9 that $TiO_2$/C and N-$TiO_2$/NC samples exhibit a similar layered structure. However, the $TiO_2$/C sample exhibits very close layer-to-layer distances and tight connections between $TiO_2$ particles, which may be detrimental to the electron transfer and hydrogen evolution reactions. Compared with $TiO_2$/C, the N-$TiO_2$/NC sample shows a more dispersed layer structure and particle distribution. To analyze the effects of nitriding temperature and oxidation temperature, wecarried out a series of experiments and corresponding tests. The nitriding temperature of MXene is adjusted to 300 and 600 °C (450 °C in this study). SEM, XRD, and XPS tests are also used to characterize their microstructure. When the nitriding temperature is 300 °C, the interplanar spacing is enlarged (Figure S10c) and the morphology is not changed (Figure S10a), but the content of N element is less (Table S4). When the nitriding temperature is 600 °C, the (002) crystal plane corresponding to the interlayer distance disappears and it can also be observed in the SEM image, which is very unfavorable to the formation of the layered structure after oxidation. Experiments of different N-MXene oxidation temperatures (400 and 660 °C) were carried out by us. It can be found from XRD results (Figure S11a) that N-$TiO_2$/NC-400 °C may contain unreacted N-MXene. As shown in Figure S11c, $TiO_2$ particles in the N-$TiO_2$/NC-660 °C are very large, which has negative effects on the electron transport ability and photocatalytic performance. Therefore, the nitriding temperature and the oxidation temperature were preferentially selected as 450 and 530 °C, respectively, in this study.

To further analyze N-doped composite, XRD, XPS, Raman spectroscopy, and EDX elemental mapping measurements are performed. Figure 2a displays the XRD patterns of $TiO_2$/C and N-$TiO_2$/NC obtained by oxidation treatment of $Ti_3C_2T_x$ and N−$Ti_3C_2T_x$. From them, the distinct diffraction peaks of anatase $TiO_2$ can be observed in $TiO_2$/C and N-$TiO_2$/NC samples. Remarkably, it is also observed that the diffraction peaks of N-$TiO_2$/NC have slight shifts compared with $TiO_2$/C. It can be confirmed in Figure 2b that diffraction angle of the anatase (101) plane in N-$TiO_2$/NC is decreased by 0.17° relative to $TiO_2$/C, which indicates that the interplanar distances of (101) are expanded. Moreover, it is found that other crystal faces of anatase for N-$TiO_2$/NC sample also have different degrees toward low angle (Figure S12). This may imply that nitrogen with a larger atomic radius acts as dopant in the $TiO_2$ crystal, leading to lattice expansion.[44,45] As shown in N 1s XPS spectra of two samples (Figure 2c), the presence of nitrogen species is confirmed, and the obvious peaks at 398.7 and 401.0 eV are observed in N-$TiO_2$/NC, in comparison to $TiO_2$/C. The position at 401.0 eV in the N 1s XPS spectrum of N-$TiO_2$/NC (Figure 2c) should be attributed to the Ti−O−N bond formed by interstitial N atom.[46,47] It directly proves that nitrogen has been successfully introduced into $TiO_2$ crystal. N-doping of $TiO_2$ is also proved from Raman spectra, Ti 2p and O 1s XPS spectra (Figure 2d and Figure S13a, b). It can be seen in Raman spectra (Figure 2d) that the characteristic peaks at 388, 506, and 625 $cm^{-1}$ of the $TiO_2$/C and N-$TiO_2$/NC ascribe to $B_{1g}$, $A_{1g}$ + $B_{1g}$ and $E_g$ vibrations of anatase $TiO_2$, respectively.[48] Interestingly, as shown in the inset (Figure 2d), the peak at 141 $cm^{-1}$ originally located in $TiO_2$/C, slightly shifts to high frequency, implying the change in electron density owing to N-doping. Figure S13a, b exhibit Ti 2p and O 1s XPS spectra of the $TiO_2$/C and N-$TiO_2$/NC. It is clearly found that the binding energy of Ti and O in N-$TiO_2$/NC shifts toward negative direction compared with unmodified $TiO_2$/C. This is due to the formation of Ti−O−N bond attributed to the introduction of nitrogen. Because the electronegativity of oxygen is higher than that of nitrogen, the electron cloud of the nitrogen atom is biased toward the oxygen atom, which increases the electron cloud density near the oxygen. This leads to a decrease in the oxygen binding energy. In addition, doping of nitrogen weakens Ti−O bond, which results in a decrease in the binding force of Ti and O. The locations at 458.3, 464.0, 529.9, and 531.8 eV are attributed to Ti $2p_{3/2}$, Ti $2p_{1/2}$, O−Ti−O bond and O−H bond of N-$TiO_2$/NC, respectively (inset in Figure S8a, b). In addition, other peaks were not found in the Ti and O XPS spectra of two samples.

A typical peak at 398.7 eV in N 1s spectra (Figure 2c) should be assigned to pyridinic N.[49] Pyridinic N-doped carbon can greatly enhance its electron transport ability and catalytic performance.[50,51] As exhibited in the C 1s XPS spectra, $TiO_2$/C and N-$TiO_2$/NC share peaks at 284.8, 287.0, and 288.6 eV together, which are attributed to C═C bond (standard peak), C−O bond, and O−C═O bond respectively. Interestingly, the peak located at 286.2 eV (Figure 2e), which ascribes to C═N, can be only observed in N-$TiO_2$/NC sample, agreed with its N 1s spectra.[52] The above results are also proved by the Raman spectra (Figure S14). The Raman peaks at 1385 and 1580 $cm^{-1}$, which represent defects and in-plane vibrations of carbon atoms hybridized by $sp^2$, respectively, manifest the formation of carbon, and we generally calculate the value of $I_D/I_G$ to reflect the degree of carbon deficiency. It is found that the $I_D/I_G$ value (0.80) for N-$TiO_2$/NC is higher than that of $TiO_2$/C (0.71), which means that the former contains more defects and implies that nitrogen atoms are doped into the carbon. Carbon content in the N-$TiO_2$/NC sample by TG analysis (Figure S15) is about 6%. It is observed from the EDX analysis results of N-$TiO_2$/NC (Figure S16) that the existence of N species is confirmed. Afterward, as shown in the SEM image and corresponding elemental mapping and HAADF-STEM image and corresponding EDS elemental graphs of N-$TiO_2$/NC (Figure S17 and Figure 2f−i), it can be clearly seen that the N element is uniformly distributed in $TiO_2$ and the carbon layer of N-$TiO_2$/NC. The same phenomenon is also observed in Ti, O, and C elements. The EDS mapping and graphs provide a direct proof that heterogeneous nitrogen atoms have been successfully introduced into $TiO_2$ and carbon, respectively.

To further study the morphology and microstructure of as-obtained N-$TiO_2$/NC sample, SEM, TEM and HRTEM


https://dx.doi.org/10.1021/acsanm.9b02217
ACS Appl. Nano Mater. 2020, 3, 1373−1381

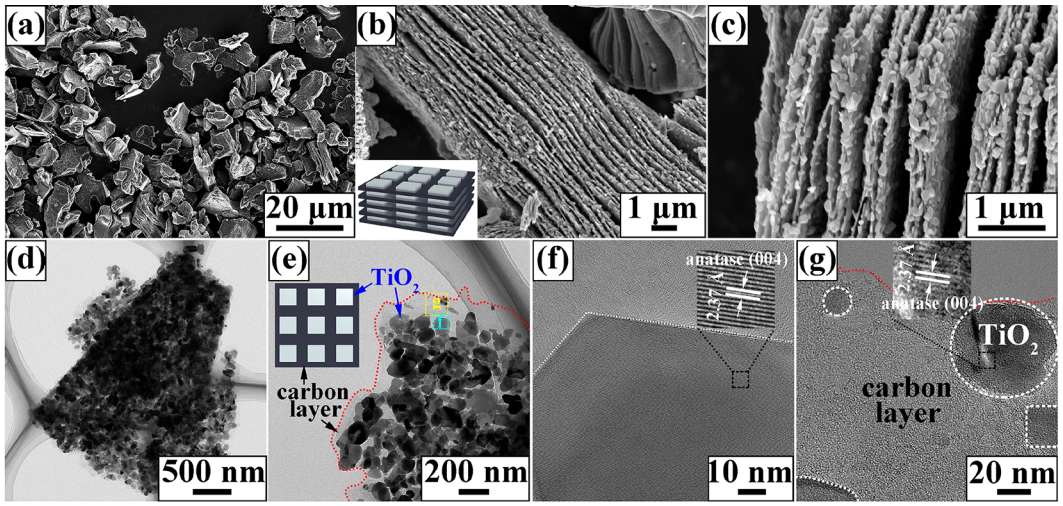


**Figure 3.** (a–c) SEM images, and (d, e) TEM images, and (f, g) HRTEM images of N-$TiO_2$/NC sample.

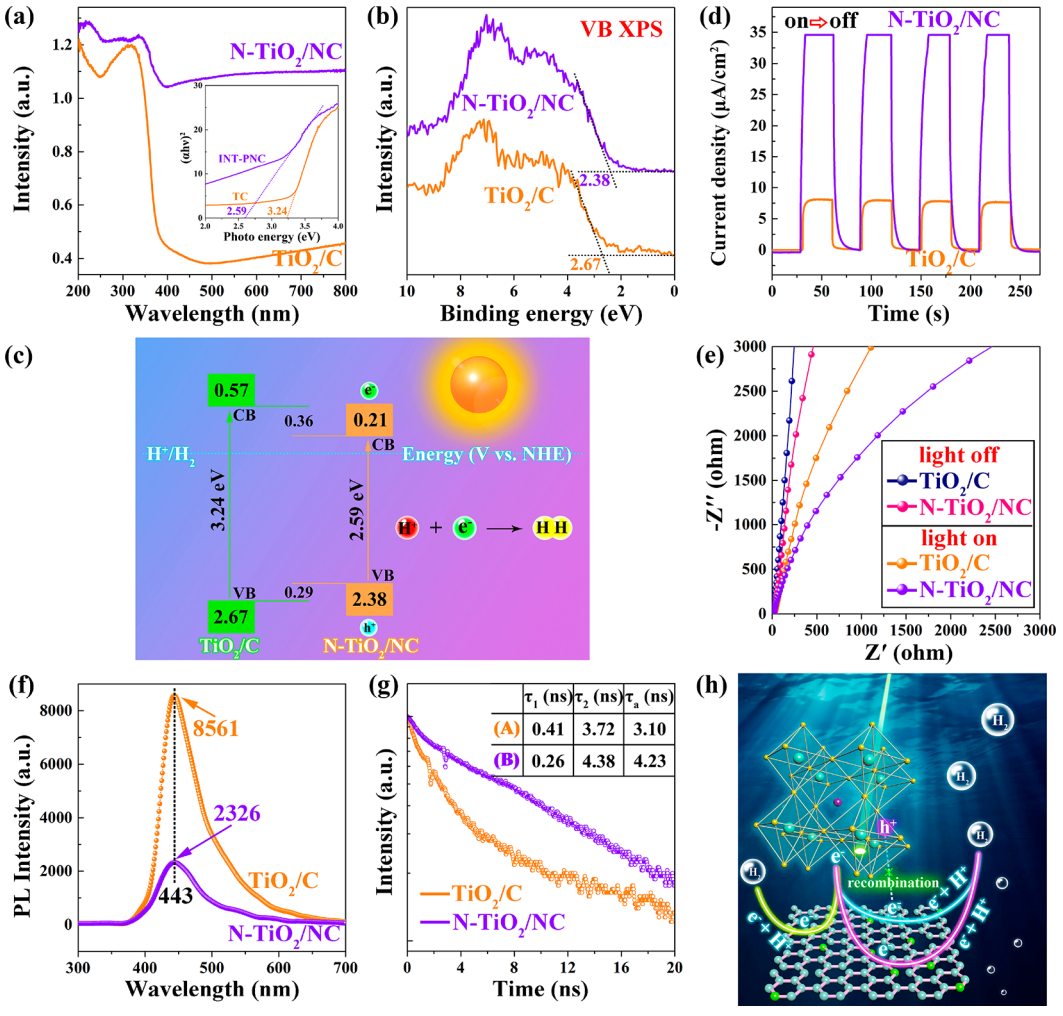


**Figure 4.** Optical and electrical measurements of the $TiO_2$/C and N-$TiO_2$/NC samples: (a) UV–vis DRS and their corresponding Tauc/Davis–Mott plots in the inset. (b, c) VB XPS spectra and the band gap structures. (d, e) Transient photocurrent density curves and EIS Nyquist plots under dark and light irradiation. (f, g) Photoluminescence emission curves and time-resolved transient PL decay curves. (h) Photocatalytic schematic diagram of N-$TiO_2$/NC heterostructure.

measurements are conducted. As shown in SEM images (Figure 3a-c and S18a, b) that the sample still maintains a preferable layered structure similar to pristine N-MXene. It can also be observed that many cuboid-like nanoparticles (length/width <100 nm) with thin thickness are neatly and evenly distributed on a typical layer, which is also confirmed by its



https://dx.doi.org/10.1021/acsanm.9b02217
ACS Appl. Nano Mater. 2020, 3, 1373–1381

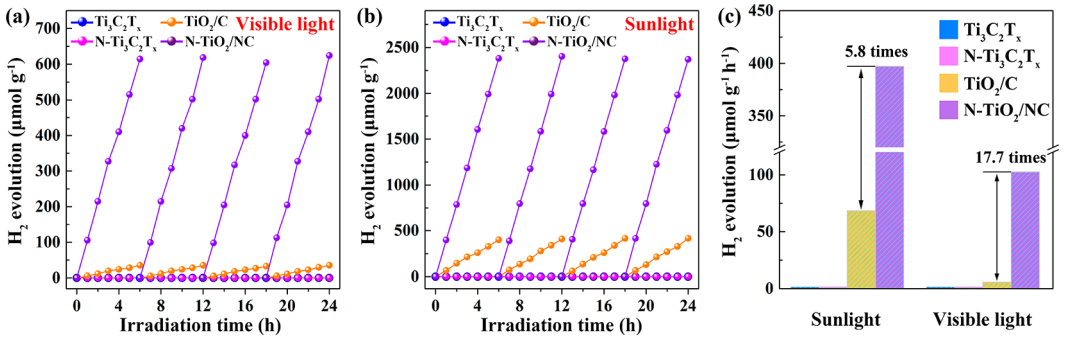


**Figure 5.** Typical time course of hydrogen evolution for $Ti_3C_2T_x$, $N-Ti_3C_2T_x$, and $TiO_2/C$ and $N\text{-}TiO_2/NC$ samples under (a) visible light and (b) simulated sunlight. (c) Average hydrogen production rates of four samples.

TEM image (Figure 3d). In order to identify the nanocrystal composition, we treated the sample under strong ultrasound conditions for a long time, as shown in Figure 3e and Figure S12c–e. It is clearly seen from its HRTEM (Figure 3f, g) that the interplanar spacing is 2.37 Å, which matches well with the (004) crystal plane of anatase. The results also show that the (001) plane is the main exposed plane of titanium dioxide above the sheet. And its SEAD pattern (Figure S19) also verifies that the nanoparticles contain only anatase $TiO_2$ phase, agreed with the XRD results. From the above results, the obtained $N\text{-}TiO_2/NC$ sample presents a laminated structure decorated with cuboid-like $TiO_2$ nanocrystals with exposing the (004) crystal plane. The specific surface area (SSA) and pore structure for $TiO_2/C$ and $N\text{-}TiO_2/NC$ samples are analyzed by Brunauer–Emmett–Teller (BET) measurement, as illustrated in Figure S20. As shown in Figure S20a, compared with SSA of $TiO_2/C$ (63.26 $m^2\ g^{-1}$), the $N\text{-}TiO_2/NC$ sample exhibits a larger SSA (70.68 $m^2\ g^{-1}$), which is beneficial to expose more active sites. It is observed that the two samples have similar pore structures and their pore sizes are widely distributed at 5–150 nm.

The UV–vis DRS examinations were conducted to investigate the light absorption performance and band structures of $TiO_2/C$ and $N\text{-}TiO_2/NC$ photocatalysts. It is clearly found from Figure 4a that the light absorption of $N\text{-}TiO_2/NC$ is dramatically enhanced in the wavelength range of 400–800 nm, which is owing to synergistic effect of N-doping of $TiO_2$ and optimized electronic structure of carbon induced by N-doping. More importantly, based on the transformed plot of UV–vis DRS by Kubelka–Munk formula, the band gaps of $TiO_2/C$ and $N\text{-}TiO_2/NC$ are evaluated as 3.24 and 2.59 eV (inset of Figure 4a), respectively. The narrowed band gap of the $N\text{-}TiO_2/NC$ sample is mainly due to the appearance of heterogeneous nitrogen, which leads to a red shift to visible light. It can be observed from the valence band (VB) spectra (Figure 4b) that the VB top of $TiO_2/C$ and $N\text{-}TiO_2/NC$ are 2.67 and 2.38 eV, respectively. Therefore, their conduction band (CB) positions and energy band structures can be determined, as exhibited in Figure 4c.

To investigate the ability of charge transportation and separation in the $TiO_2/C$ and $N\text{-}TiO_2/NC$ photocatalysts, transient photocurrent, electrochemical impedance, photoluminescence (PL) and fluorescence lifetime examinations have been carried out. The photocurrent response of two hybrids are performed first. As illustrated in Figure 4d, the transient photocurrent density of $N\text{-}TiO_2/NC$ is up to 34.6 $\mu A\ cm^{-2}$, which is approximately 4.3 times higher than that of $TiO_2/C$ (8.1 $\mu A\ cm^{-2}$). The outstanding performance can serve as a proof that $N\text{-}TiO_2/NC$ heterostructure can strongly realize visible light absorption and efficiently accelerate the transportation and separation of carriers due to N-doping of $TiO_2$ and superior conductivity induced by N-doped carbon. Their conductivity is analyzed by electrochemical impedance tests under dark and light irradiation, as shown in Figure 4e. The arc radii in the semicircular Nyquist plots of $N\text{-}TiO_2/NC$ sample (Figure 4e) are much smaller under light on and off than those of $TiO_2/C$, certifying optimized transportation and separation efficiency of electrons and holes in $N\text{-}TiO_2/NC$, which is consistent with the photocurrent results.[53] More importantly, the former's impedance in the absence of light strongly shows its exceptional ability for electron transmission relative to the latter, which is due to N-doping of carbon. To further identify the separation efficiency of carriers, were later carried out PL examinations. The PL intensity of $TiO_2/C$ (8561 cps) is quite higher at the 320 nm excitation wavelength than that of $N\text{-}TiO_2/NC$ sample (2326 cps), which reveals the lower recombination ratio of electron–holes in $N\text{-}TiO_2/NC$ (Figure 4f). The result of PL tests demonstrates that the $N\text{-}TiO_2/NC$ heterostructure enable efficient separation of photoinduced electron–holes compared with unmodified $TiO_2/C$. The separation ability of carriers for two samples also is illustrated by fluorescence lifetime analysis (Figure 4g, Figure S21 and Table S5). The short life $\tau_1$ and long life $\tau_2$ are derived from the nonradiative recombination and the interband recombination of the free-excitons on $TiO_2$ nanoparticles.[54−56] Compared with undoped $TiO_2/C$ ($\tau_a$ = 3.10 ns), the $N\text{-}TiO_2/NC$ hybrid has a long average fluorescent lifetime ($\tau_a$ = 4.23 ns), which indicates that the carrier lifetime in the doped sample is prolonged and recombination of carrier is effectively suppressed. All the above results demonstrate that the $N\text{-}TiO_2/NC$ heterostructure dramatically accelerates the electron transfer and effectively promotes the separation of electron–holes, which are boost to its photocatalytic activity. The photocatalytic schematic diagram of $N\text{-}TiO_2/NC$ heterostructure is illustrated in Figure 4h.

We performed the measurements of hydrogen generation to examine the photocatalytic activity of as-obtained samples. It can be observed from Figure 5a and b that almost no hydrogen is released in $Ti_3C_2T_x$ and $N-Ti_3C_2T_x$ systems during the light irradiation. However, the samples after oxidation have a significant change in hydrogen production under light condition. The average production rates of $H_2$ (Figure 5c) for $N\text{-}TiO_2/NC$ heterostructure under visible light and simulated sunlight irradiation without any cocatalyst reach up to 102.6 and 397.1 $\mu mol\ g^{-1}\ h^{-1}$ respectively, which are


https://dx.doi.org/10.1021/acsanm.9b02217
ACS Appl. Nano Mater. 2020, 3, 1373–1381

about 17.7 and 5.8 times higher than those of $TiO_2$/C (ca. 5.8 and 67.8 $\mu$mol $g^{-1}$ $h^{-1}$). This result certifies that N-$TiO_2$/NC hybrid has an admirable photocatalytic performance under visible light compared to unmodified $TiO_2$/C sample. In addition, the photocatalytic hydrogen production tests (Figures S22 and 23) of P25-$TiO_2$ and N-$TiO_2$ (long-term oxidation of N-$TiO_2$/NC sample) were also carried out, and their hydrogen production was 0.94 and 13.5 $\mu$mol $g^{-1}$ $h^{-1}$, respectively. For comparative analysis, many N-doped or composite photocatalysts and their photocatalytic performance are also listed in Table S6. Meanwhile, the layered heterostructure N-$TiO_2$/NC photocatalyst still maintains an outstanding generation rate of $H_2$ (ca. 102 $\mu$mol $g^{-1}$ $h^{-1}$) with robust stability after recycling for 120 h under visible light (Figure S24). In addition, no obvious changes are observed in the morphology and composition of N-$TiO_2$/NC sample after stability tests, as displayed in Figure S25.

## 4. CONCLUSIONS

In conclusion, we have rationally designed and fabricated a nanolayered heterostructure based on N-doped $TiO_2$ and N-doped carbon by a novel method. Furthermore, the as-obtained N-$TiO_2$/NC nanohybird photocatalyst can robustly absorb visible light and effectively separate electron−holes owing to N-doping of $TiO_2$ and carbon. Therefore, the N-$TiO_2$/NC photocatalyst with nanolayered heterostructure could efficiently split water under visible light with a prominent $H_2$ evolution rate up to 102.6 $\mu$mol $g^{-1}$ $h^{-1}$ (17.7 times higher than that of $TiO_2$/C). Realization of two different types of N-doping based on N-MXene sheds a new approach for the doping of semiconductor nanoheterostructure.

## ■ ASSOCIATED CONTENT

### Supporting Information

The Supporting Information is available free of charge at https://pubs.acs.org/doi/10.1021/acsanm.9b02217.

SEM and TEM images; C 1s, Ti 2p, and O 1s XPS spectra;, pristine image of N−$Ti_3C_2T_x$; EDS mappings; XRD patterns; FT-IR spectra and Raman spectra of samples; S; TG curve of the N-$TiO_2$/NC sample; EDX spectrum and corresponding element contents of N-$TiO_2$/NC; SAED pattern of N-$TiO_2$/NC; $N_2$ adsorption/desorption isotherms and pore size distribution curves of samples; time-resolved transient PL decay curves of samples; typical time courses of hydrogen evolution; N 1s core level peak analyses; atomic concentration (at %); C 1s core level peak analyses; values of TRPL lifetime $\tau_i$ and corresponding constant $A_i$; performance comparisons with other studies (PDF)

## ■ AUTHOR INFORMATION


### Corresponding Authors

**Piaoping Yang** − *College of Materials Science and Chemical Engineering, Harbin Engineering University, Harbin, Heilongjiang 150001, P. R. China;* orcid.org/0000-0002-9555-1803; Email: yangpiaoping@hrbeu.edu.cn

**Wei Ye** − *College of Material, Chemistry and Chemical Engineering, Hangzhou Normal University, Hangzhou, Zhejiang 311121, P. R. China*; Email: yewei@hznu.edu.cn

**Peng Gao** − *College of Materials Science and Chemical Engineering, Harbin Engineering University, Harbin, Heilongjiang 150001, P. R. China; College of Material, Chemistry and Chemical Engineering, Hangzhou Normal University, Hangzhou, Zhejiang 311121, P. R. China;* orcid.org/0000-0002-8742-2833; Email: gaopeng@hrbeu.edu.cn

### Authors

**Xianglong Kong** − *College of Materials Science and Chemical Engineering, Harbin Engineering University, Harbin, Heilongjiang 150001, P. R. China*

**Zhenbo Peng** − *Zhejiang Collaborative Innovation Center for High Value Utilization of Byproducts from Ethylene Project, Ningbo Polytechnic, Ningbo, Zhejiang 315800, P. R. China*

**Rui Jiang** − *College of Materials Science and Chemical Engineering, Harbin Engineering University, Harbin, Heilongjiang 150001, P. R. China*

**Peipei Jia** − *College of Materials Science and Chemical Engineering, Harbin Engineering University, Harbin, Heilongjiang 150001, P. R. China*

**Jing Feng** − *College of Materials Science and Chemical Engineering, Harbin Engineering University, Harbin, Heilongjiang 150001, P. R. China;* orcid.org/0000-0001-5997-828X

**Qianqian Chi** − *College of Material, Chemistry and Chemical Engineering, Hangzhou Normal University, Hangzhou, Zhejiang 311121, P. R. China*

**Fuchun Xu** − *College of Material, Chemistry and Chemical Engineering, Hangzhou Normal University, Hangzhou, Zhejiang 311121, P. R. China*

Complete contact information is available at: https://pubs.acs.org/10.1021/acsanm.9b02217

### Author Contributions

These authors contributed equally to this work.


### Notes

The authors declare no competing financial interest.

## ■ ACKNOWLEDGMENTS

This work was financially supported in part by the Pandeng Plan Foundation (4095C5021820406, 4095C5021820441) of Hangzhou Normal University, Natural Science Foundation of Zhejiang Provincial Natural Science Foundation (LY18E020010, LQ19B010001, LGJ20E020001), National College Students' Science and Technology Innovation Project (201910346045, 201910346038,201910346030), National Natural Science Foundation of China (51902077), Zhejiang Province "Ten Thousand People Plan", Agricultural and Social Development Program Project (20191203B03) of Hangzhou Science and Technology Bureau of Zhejiang Province, and general items of Zhejiang Provincial Department of Education (Y201840068, Y201533640).

## ■ REFERENCES

(1) Chen, S.; Takata, T.; Domen, K. Particulate photocatalysts for overall water splitting. *Nat. Rev. Mater.* **2017**, *2*, 17050.

(2) Shi, N.; Li, X.; Fan, T.; Zhou, H.; Ding, J.; Zhang, D.; Zhu, H. Biogenic N-I-codoped $TiO_2$ photocatalyst derived from kelp for efficient dye degradation. *Energy Environ. Sci.* **2011**, *4*, 172−180.

(3) Wang, X.; Wang, F.; Sang, Y.; Liu, H. Full-spectrum solar-light-activated photocatalysts for light-chemical energy conversion. *Adv. Energy Mater.* **2017**, *7*, 1700473.

(4) Ma, Y.; Wang, X.; Jia, Y.; Chen, X.; Han, H.; Li, C. Titanium dioxide-based nanomaterials for photocatalytic fuel generations. *Chem. Rev.* **2014**, *114*, 9987−10043.

(5) Zhang, H.; Banfield, J. F. Structural characteristics and mechanical and thermodynamic properties of nanocrystalline $TiO_2$. *Chem. Rev.* **2014**, *114*, 9613−9644.
(6) Iwashina, K.; Iwase, A.; Ng, Y. H.; Amal, R.; Kudo, A. Z-schematic water splitting into $H_2$ and $O_2$ using metal sulfide as a hydrogen-evolving photocatalyst and reduced graphene oxide as a solid-state electron mediator. *J. Am. Chem. Soc.* **2015**, *137*, 604−607.
(7) Kudo, A.; Miseki, Y. Heterogeneous photocatalyst materials for water splitting. *Chem. Soc. Rev.* **2009**, *38*, 253−278.
(8) Li, P. Q.; Hu, H. T.; Xu, J. F.; Jing, H.; Peng, H.; Lu, J.; Wu, C. X.; Ai, S. Y. New insights into the photo-enhanced electrocatalytic reduction of carbon dioxide on $MoS_2$-rods/$TiO_2$ NTs with unmatched energy band. *Appl. Catal., B* **2014**, *147*, 912−919.
(9) Zhang, J.; Xu, Q.; Feng, Z.; Li, M.; Li, C. Importance of the relationship between surface phases and photocatalytic activity of $TiO_2$. *Angew. Chem., Int. Ed.* **2008**, *47*, 1766−1769.
(10) Park, J. H.; Kim, S.; Bard, A. J. Novel carbon-doped $TiO_2$ nanotube arrays with high aspect ratios for efficient solar water splitting. *Nano Lett.* **2006**, *6*, 24−28.
(11) Zhao, Z. H.; Tian, J.; Sang, Y. H.; Cabot, A.; Liu, H. Structure, synthesis, and applications of tio$_2$ nanobelts. *Adv. Mater.* **2015**, *27*, 2557−2582.
(12) Sun, J.; Yang, Y.; Khan, J. I.; Alarousu, E.; Guo, Z.; Zhang, X.; Zhang, Q.; Mohammed, O. F. Ultrafast carrier trapping of a metal-doped titanium dioxide semiconductor revealed by femtosecond transient absorption spectroscopy. *ACS Appl. Mater. Interfaces* **2014**, *6*, 10022−10027.
(13) Khan, S. U.; Al-Shahry, M.; Ingler, W. B., Jr. Efficient photochemical water splitting by a chemically modified n-$TiO_2$. *Science* **2002**, *297*, 2243−2245.
(14) Liu, G.; Yang, H. G.; Wang, X. W.; Cheng, L. N.; Pan, J.; Lu, G. Q.; Cheng, H. M. Visible light responsive nitrogen doped anatase $TiO_2$ sheets with dominant {001} facets derived from TiN. *J. Am. Chem. Soc.* **2009**, *131*, 12868−12869.
(15) Asahi, R.; Morikawa, T.; Ohwaki, T.; Aoki, K.; Taga, Y. Visible-light photocatalysis in nitrogen-doped titanium oxides. *Science* **2001**, *293*, 269−271.
(16) Nam, S.-H.; Kim, T. K.; Boo, J.-H. Physical property and photo-catalytic activity of sulfur doped $TiO_2$ catalysts responding to visible light. *Catal. Today* **2012**, *185*, 259−262.
(17) Livraghi, S.; Paganini, M. C.; Giamello, E.; Selloni, A.; Di Valentin, C.; Pacchioni, G. Origin of photoactivity of nitrogen-doped titanium dioxide under visible light. *J. Am. Chem. Soc.* **2006**, *128*, 15666−15671.
(18) Wang, Y.; Feng, C.; Zhang, M.; Yang, J.; Zhang, Z. Enhanced visible light photocatalytic activity of N-doped $TiO_2$ in relation to single-electron-trapped oxygen vacancy and doped-nitrogen. *Appl. Catal., B* **2010**, *100*, 84−90.
(19) Jagadale, T. C.; Takale, S. P.; Sonawane, R. S.; Joshi, H. M.; Patil, S. I.; Kale, B. B.; Ogale, S. B. N-Doped $TiO_2$ nanoparticle based visible light photocatalyst by modified peroxide sol-gel method. *J. Phys. Chem. C* **2008**, *112*, 14595−14602.
(20) Xu, H.; Ouyang, S.; Liu, L.; Reunchan, P.; Umezawa, N.; Ye, J. Recent advances in $TiO_2$-based photocatalysis. *J. Mater. Chem. A* **2014**, *2*, 12642−12661.
(21) Tao, J.; Luttrell, T.; Batzill, M. A two-dimensional phase of $TiO_2$ with a reduced bandgap. *Nat. Chem.* **2011**, *3*, 296−300.
(22) Xiang, Q.; Yu, J.; Jaroniec, M. Synergetic effect of $MoS_2$ and graphene as cocatalysts for enhanced photocatalytic $H_2$ production activity of $TiO_2$ nanoparticles. *J. Am. Chem. Soc.* **2012**, *134*, 6575−6578.
(23) Bonaccorso, F.; Colombo, L.; Yu, G.; Stoller, M.; Tozzini, V.; Ferrari, A. C.; Ruoff, R. S.; Pellegrini, V. 2D materials. Graphene, related two-dimensional crystals, and hybrid systems for energy conversion and storage. *Science* **2015**, *347*, 1246501.
(24) Xie, G.; Zhang, K.; Guo, B.; Liu, Q.; Fang, L.; Gong, J. R. Graphene-based materials for hydrogen generation from light-driven water splitting. *Adv. Mater.* **2013**, *25*, 3820−39.
(25) Zhang, K.; Zhao, Y.; Fu, D.; Chen, Y. Molybdenum carbide nanocrystal embedded N-doped carbon nanotubes as electrocatalysts for hydrogen generation. *J. Mater. Chem. A* **2015**, *3*, 5783−5788.
(26) Yuan, X.; Zhang, M.; Chen, X.; An, N.; Liu, G.; Liu, Y.; Zhang, W.; Yan, W.; Jia, M. Transesterification of dimethyl oxalate with phenol over nitrogen-doped nanoporous carbon materials. *Appl. Catal., A* **2012**, *439*−*440*, 149−155.
(27) Xu, X.; Lai, L.; Jiang, J. H.; He, Z. Q.; Song, S. C,N-codoped $TiO_2$ with a nitrogen-doped carbon coating derived from 2,6-Diaminopyridine for visible light-induced photocatalytic hydrogen evolution. *J. Phys. Chem. C* **2019**, *123*, 9702−9712.
(28) Yu, J. Y.; Zhou, W. J.; Xiong, T. L.; Wang, A. L.; Chen, S. W.; Chu, B. L. Enhanced electrocatalytic activity of Co@N-doped carbon nanotubes by ultrasmall defect-rich $TiO_2$ nanoparticles for hydrogen evolution reaction. *Nano Res.* **2017**, *10*, 2599−2609.
(29) Shi, R.; Li, Z.; Yu, H. J.; Shang, L.; Zhou, C.; Waterhouse, G. I. N.; Wu, L. Z.; Zhang, T. R. Effect of nitrogen doping level on the performance of N-doped carbon quantum dot/$TiO_2$ composites for photocatalytic hydrogen evolution. *ChemSusChem* **2017**, *10*, 4650−4656.
(30) Anasori, B.; Lukatskaya, M. R.; Gogotsi, Y. 2D metal carbides and nitrides (MXenes) for energy storage. *Nat. Rev. Mater.* **2017**, *2*, 16098.
(31) Seh, Z. W.; Fredrickson, K. D.; Anasori, B.; Kibsgaard, J.; Strickler, A. L.; Lukatskaya, M. R.; Gogotsi, Y.; Jaramillo, T. F.; Vojvodic, A. Two-dimensional molybdenum carbide (MXene) as an efficient electrocatalyst for hydrogen evolution. *ACS Energy Lett.* **2016**, *1*, 589−594.
(32) Ran, J.; Gao, G.; Li, F. T.; Ma, T. Y.; Du, A.; Qiao, S. Z. $Ti_3C_2$ MXene co-catalyst on metal sulfide photo-absorbers for enhanced visible-light photocatalytic hydrogen production. *Nat. Commun.* **2017**, *8*, 13907.
(33) Ghidiu, M.; Lukatskaya, M. R.; Zhao, M. Q.; Gogotsi, Y.; Barsoum, M. W. Conductive two-dimensional titanium carbide 'clay' with high volumetric capacitance. *Nature* **2014**, *516*, 78−81.
(34) Hu, M.; Hu, T.; Li, Z.; Yang, Y.; Cheng, R.; Yang, J.; Cui, C.; Wang, X. Surface functional groups and interlayer water determine the electrochemical capacitance of $Ti_3C_2T_x$ MXene. *ACS Nano* **2018**, *12*, 3578−3586.
(35) Wen, Y.; Rufford, T. E.; Chen, X.; Li, N.; Lyu, M.; Dai, L.; Wang, L. Nitrogen-doped $Ti_3C_2T_x$ MXene electrodes for high-performance supercapacitors. *Nano Energy* **2017**, *38*, 368−376.
(36) Tang, Y.; Zhu, J.; Wu, W.; Yang, C.; Lv, W.; Wang, F. Synthesis of nitrogen-doped two-dimensional $Ti_3C_2$ with enhanced electrochemical performance. *J. Electrochem. Soc.* **2017**, *164*, A923−A929.
(37) Yang, C.; Que, W.; Yin, X.; Tian, Y.; Yang, Y.; Que, M. Improved capacitance of nitrogen-doped delaminated two-dimensional titanium carbide by urea-assisted synthesis. *Electrochim. Acta* **2017**, *225*, 416−424.
(38) Li, Y. J.; Ding, L.; Guo, Y. C.; Liang, Z. Q.; Cui, H. Z.; Tian, J. Boosting the Photocatalytic Ability of g-$C_3N_4$ for Hydrogen Production by $Ti_3C_2$ MXene Quantum Dots. *ACS Appl. Mater. Interfaces* **2019**, *11*, 41440−41447.
(39) Li, Y. J.; Deng, X. T.; Tian, J.; Liang, Z. Q.; Cui, H. Z. $Ti_3C_2$ MXene-derived $Ti_3C_2$/$TiO_2$ nanoflowers for noble-metal-free photocatalytic overall water splitting. *Appl. Mater. Today* **2018**, *13*, 217−227.
(40) Li, Y. J.; Yin, Z. H.; Ji, G. R.; Liang, Z. Q.; Xue, Y. J.; Guo, Y. C.; Tian, J.; Wang, X. Z.; Cui, H. Z. 2D/2D/2D heterojunction of $Ti_3C_2$ MXene/$MoS_2$ nanosheets/$TiO_2$ nanosheets with exposed (001) facets toward enhanced photocatalytic hydrogen production activity. *Appl. Catal., B* **2019**, *246*, 12−20.
(41) Li, Y. J.; Yang, S. R.; Liang, Z. Q.; Xue, Y. J.; Cui, H. Z.; Tian, J. 1T-$MoS_2$ nanopatch/$Ti_3C_2$ MXene/$TiO_2$ nanosheet hybrids for efficient photocatalytic hydrogen evolution. *Mater. Chem. Front* **2019**, *3*, 2673−2680.
(42) Peng, C.; Wei, P.; Li, X. Y.; Liu, Y. P.; Cao, Y. H.; Wang, H. J.; Yu, H.; Peng, F.; Zhang, L. Y.; Zhang, B. S.; Lv, K. L. High efficiency photocatalytic hydrogen production over ternary Cu/$TiO_2$@$Ti_3C_2T_x$


https://dx.doi.org/10.1021/acsanm.9b02217
*ACS Appl. Nano Mater.* 2020, 3, 1373−1381

enabled by low-work-function 2D titanium carbide. *Nano Energy* **2018**, *53*, 97−107.
(43) Peng, C.; Xu, W. K.; Wei, P.; Liu, M. C.; Guo, L.; Wu, P. P.; Zhang, K.; Cao, Y. H.; Wang, H. J.; Yu, H.; Peng, F.; Yan, X. Q. Manipulating photocatalytic pathway and activity of ternary $Cu_2O$/(001)$TiO_2$@$Ti_3C_2T_x$ catalysts for $H_2$ evolution: Effect of surface coverage. *Int. J. Hydrogen Energy* **2019**, *44*, 29975−29985.
(44) Sun, S.; Gao, P.; Yang, Y.; Yang, P.; Chen, Y.; Wang, Y. N-doped $TiO_2$ nanobelts with coexposed (001) and (101) facets and their highly efficient visible-light-driven photocatalytic hydrogen production. *ACS Appl. Mater. Interfaces* **2016**, *8*, 18126−18131.
(45) Cheng, J.; Chen, J.; Lin, W.; Liu, Y.; Kong, Y. Improved visible light photocatalytic activity of fluorine and nitrogen co-doped $TiO_2$ with tunable nanoparticle size. *Appl. Surf. Sci.* **2015**, *332*, 573−580.
(46) Ananpattarachai, J.; Kajitvichyanukul, P.; Seraphin, S. Visible light absorption ability and photocatalytic oxidation activity of various interstitial N-doped $TiO_2$ prepared from different nitrogen dopants. *J. Hazard. Mater.* **2009**, *168*, 253−261.
(47) Gu, D.-E.; Yang, B.-C.; Hu, Y.-D. V and N co-doped nanocrystal anatase $TiO_2$ photocatalysts with enhanced photocatalytic activity under visible light irradiation. *Catal. Commun.* **2008**, *9*, 1472−1476.
(48) Jo, W.-K.; Kumar, S.; Isaacs, M. A.; Lee, A. F.; Karthikeyan, S. Cobalt promoted $TiO_2$/GO for the photocatalytic degradation of oxytetracycline and Congo Red. *Appl. Catal., B* **2017**, *201*, 159−168.
(49) Yang, Y.; Lun, Z.; Xia, G.; Zheng, F.; He, M.; Chen, Q. Non-precious alloy encapsulated in nitrogen-doped graphene layers derived from MOFs as an active and durable hydrogen evolution reaction catalyst. *Energy Environ. Sci.* **2015**, *8*, 3563−3571.
(50) Luo, Z.; Lim, S.; Tian, Z.; Shang, J.; Lai, L.; MacDonald, B.; Fu, C.; Shen, Z.; Yu, T.; Lin, J. Pyridinic N doped graphene: synthesis, electronic structure, and electrocatalytic property. *J. Mater. Chem.* **2011**, *21*, 8038−8044.
(51) Wang, H.; Maiyalagan, T.; Wang, X. Review on recent progress in nitrogen-doped graphene: synthesis, characterization, and its potential applications. *ACS Catal.* **2012**, *2*, 781−794.
(52) Xu, Y.; Mo, Y.; Tian, J.; Wang, P.; Yu, H.; Yu, J. The synergistic effect of graphitic N and pyrrolic N for the enhanced photocatalytic performance of nitrogen-doped graphene/$TiO_2$ nanocomposites. *Appl. Catal., B* **2016**, *181*, 810−817.
(53) Mao, C.; Zuo, F.; Hou, Y.; Bu, X.; Feng, P. In situ preparation of a $Ti^{3+}$ self-doped $TiO_2$ film with enhanced activity as photoanode by $N_2H_4$ reduction. *Angew. Chem., Int. Ed.* **2014**, *53*, 10485−10489.
(54) Jia, G. R.; Wang, Y.; Cui, X. Q.; Yang, Z. X.; Liu, L. L.; Zhang, H. Y.; Wu, Q.; Zheng, L. R.; Zheng, W. T. Asymmetric embedded benzene ring enhances charge transfer of carbon nitride for photocatalytic hydrogen generation. *Appl. Catal., B* **2019**, *258*, 117959.
(55) Wang, Y.; Liu, X. Q.; Liu, J.; Han, B.; Hu, X. Q.; Yang, F.; Xu, Z. W.; Li, Y. C.; Jia, S. R.; Li, Z.; Zhao, Y. L. Carbon quantum dot implanted graphite carbon nitride nanotubes: excellent charge separation and enhanced photocatalytic hydrogen evolution. *Angew. Chem., Int. Ed.* **2018**, *57*, 5765−5771.
(56) Zhang, Z. Y.; Huang, J. D.; Fang, Y. R.; Zhang, M. Y.; Liu, K. C.; Dong, B. A nonmetal plasmonic Z-scheme photocatalyst with UV- to NIR-driven photocatalytic protons reduction. *Adv. Mater.* **2017**, *29*, 1606688.


https://dx.doi.org/10.1021/acsanm.9b02217
*ACS Appl. Nano Mater.* 2020, 3, 1373−1381